

Fluid Antenna Grouping-Based Index Modulation: Transceiver Design for MIMO Systems

Xinghao Guo, Yin Xu, *Senior Member, IEEE*, Dazhi He, *Senior Member, IEEE*, Cixiao Zhang, Wenjun Zhang, *Fellow, IEEE*, and Yiyuan Wu, *Life Fellow, IEEE*

Abstract—The fluid antenna (FA)-enabled multiple-input multiple-output (MIMO) system based on index modulation (IM), referred to as FA-IM, significantly enhances spectral efficiency (SE) compared to the conventional FA-assisted MIMO system. This paper proposes an innovative FA grouping-based IM (FAG-IM) system to improve performance in mitigating the high spatial correlation between multiple activated ports. A block grouping scheme is employed based on the spatial correlation model and the distribution structure of the ports. Then, a closed-form expression for the average bit error probability (ABEP) upper bound of the FAG-IM system is derived. In order to reduce the receiver complexity of the proposed system, the message passing mechanism is first incorporated into the FAG-IM system. Subsequently, within the approximate message passing (AMP) framework, an efficient structured AMP (S-AMP) detector is devised by leveraging the structural characteristics of the transmission signal vector. Simulation results confirm that the proposed FAG-IM system significantly outperforms the existing FA-IM system in the presence of spatial correlation. The derived ABEP curve aligns well with the numerical results, providing an efficient theoretical tool for evaluating the system performance. Additionally, simulation results demonstrate that the proposed low-complexity S-AMP detector not only reduces the time complexity to a linear scale but also substantially improves bit error rate (BER) performance compared to the minimum mean square error (MMSE) detector, thus facilitating the practical implementation of the FAG-IM system.

Index Terms—Index modulation, fluid antenna, MIMO, spatial correlation, average bit error probability, approximate message passing.

I. INTRODUCTION

WITH the rapid increase of wireless devices, future wireless communication networks are anticipated to attain higher energy efficiency and spectral efficiency (SE). Numerous key technologies, including advanced coding and modulation [1]–[3], resource allocation [4], and notably multiple-input

This work was supported in part by the National Key Research and Development Project of China under Grant 2023YFF0904603; in part by the National Natural Science Foundation of China Program under Grant 62371291, Grant 62271316, and Grant 62101322; and in part by the Fundamental Research Funds for the Central Universities and Shanghai Key Laboratory of Digital Media Processing (STCSM) under Grant 18DZ2270700. (Corresponding author: Yin Xu.)

Xinghao Guo, Yin Xu, Dazhi He, Cixiao Zhang, and Wenjun Zhang are with the Cooperative Medianet Innovation Center, Shanghai Jiao Tong University, Shanghai 200240, China (e-mail: guoxinghao, xuyin, hedazhi, cixiaozhang, zhangwenjun@sjtu.edu.cn). Dazhi He is also affiliated with Pengcheng Laboratory, Shenzhen 518055, China.

Yiyuan Wu is with the Department of Electrical and Computer Engineering, Western University, London, ON N6A 3K7, Canada (e-mail: yiyuan.wu@ieee.org).

multiple-output (MIMO) [5], have been extensively applied in various communication networks to offer enormous data speeds and stable connectivity. By deploying multiple antennas at both the transmitter and receiver, the MIMO systems, such as multi-user MIMO and massive MIMO, create multiple spatial streams for data transmission. However, traditional MIMO systems employ fixed-position antenna (FPA) arrays, which cannot fully exploit the wireless channel spatial variation within the regions of the transmitter and receiver.

An emerging and promising reconfigurable antenna technology, also known as the fluid antenna (FA) or movable antenna (MA), has been recently proposed to overcome such limitations [6], [7]. Unlike conventional FPA, FA can be controlled via software to modify its location, shape, size, or activation characteristics, thereby fully utilizing the spatial degree of freedom (DoF) [8], [9]. Similar practical implementations of this operational mechanism have already been realized using flexible conductive materials or stepper motors [10], [11]. Thanks to the significant advantage of higher spatial diversity gain, the FA system (FAS) has gained extensive research attention, primarily focused on aspects such as system performance analysis, channel modeling, and the optimal selection of locations, also known as ports. Regarding channel modeling, the Jakes model can accurately depict the spatial correlation between different ports of FAS [12]. [13] proposes a simplified block-correlation model that approximates spatial correlation through block diagonal matrices, aiming to reduce the complexity of the FAS channel model while maintaining high accuracy. The effectiveness of FAS primarily relies on selecting the most suitable port, to ensure optimal signal transmission. To achieve this objective, [14] devises a number of fast port selection algorithms based on only a few port observations. The performance of FAS in general spatially correlated channels is investigated in [15]. The position optimization algorithm for MA was proposed in [16] to enhance the performance of multiple access systems augmented by MA. [17] studies the MIMO-FAS from an information theory perspective and designs the corresponding joint optimization algorithm for port selection, beamforming, and power allocation.

As another promising technology, index modulation (IM) leverages the index of entities, such as antennas, subcarriers, time slots, etc., to convey information [18]. IM can allocate the saved transmission energy from inactive entities to active ones, improving overall performance [19]. Spatial modulation

(SM), as one of the earliest implementations of IM, selects and activates a single antenna to transmit modulated symbols based on the information bits while simultaneously eliminating inter-channel interference and avoiding antenna synchronization issues [20]. [21] significantly improves the performance of SM system through constellation optimization. The multi-user SM (MU-SM) system proposed in [22] achieves extremely high MIMO multiplexing and diversity gains, enhancing the rate, reliability, and energy efficiency of uplink transmission. However, SM systems have the following limitations: the number of transmit antennas must be a power of two, and the transmission rate grows logarithmically rather than linearly with the number of antennas. To overcome these limitations, generalized SM (GSM) is proposed in [23], where multiple transmit antennas are simultaneously activated, with bits being mapped to the indices of antenna combinations, also referred to as activation patterns. Compared to SM, GSM offers more flexible antenna configurations and higher SE. [24] provides grouping schemes for the GSM system to enhance its performance against high channel correlation.

Regarding data detection for the SM system, the optimal maximum likelihood (ML) detector performs a search over all possible transmission signal vectors, resulting in extremely high complexity. On the other hand, the linear minimum mean square error (MMSE) detector does not consider the unique structure of the transmission signal vectors, leading to issues with accuracy [25]. Consequently, a substantial number of low-complexity detectors designed explicitly for the SM system have been proposed to approximate the performance of the optimal detector. Specifically, [26] proposes a compressed sensing detection algorithm, termed the SM matching pursuit (S MMP) detector, by leveraging the sparsity of SM signals. [22] designs a low-complexity detector for the MU-SM system within a message passing framework. The challenges associated with high-dimensional integrations and the excessive number of messages in message passing can be addressed through simplification to approximate message passing (AMP) [27]. Utilizing the AMP framework, [28] proposes a generalized AMP detector (GAMPD) for the MU-SM system that simultaneously exploits the sparsity of the SM signals and their prior probability distribution. In contrast, [29] introduces a vector-form AMP detector based on the structural characteristics of SM signals, termed message passing de-quantization detector (MPDQD). Simulation results indicate that MPDQD outperforms GAMPD at the cost of increased complexity. Building upon the aforementioned work, a structured AMP (Str-AMP) detector that captures the inherent structure of SM signals is proposed in [30] for the MU-SM system. Str-AMP detector achieves performance equivalent to MPDQD while maintaining a complexity comparable to GAMPD.

FA and IM exhibit similar operational mechanisms. Thus, a natural integration has been proposed in [31], termed FA-IM, in which FA selects and activates a port based on the input bits during each transmission interval. In [32], neural network is employed to achieve fast classification of index patterns in FA-IM systems. [33] designs a port position optimization method for the FA-IM system called position IM (PIM). Based on the traditional GSM scheme, the FA-IM system

proposed in [34] applies the FA IM mechanism to MIMO systems, where multiple ports are activated simultaneously, and a portion of the input bits is mapped to the index of the port activation pattern. Compared to the MIMO-FAS system in [17], the FA-IM system presented in [34] significantly enhances SE. Moreover, simulation results indicate that FA-IM exhibits superior bit error rate (BER) performance at the same SE. However, the activation of multiple ports in [34] does not consider channel correlation, while the ports of FA are densely arranged, exhibiting a strong spatial correlation. The performance of the FA-IM-based MIMO system degrades when the channel has spatial correlation, necessitating improvements to address this issue.

To fill this gap, this paper proposes an innovative FA grouping-based IM (FAG-IM) system. The ports on the FA are evenly divided into multiple groups, with each group individually executes port index modulation and symbol modulation. Based on the spatial correlation and distribution structure characteristics of the ports, a block grouping scheme is employed, where adjacent ports with high correlation are assigned to the same group. An efficient low-complexity detector is developed to reduce the receiver complexity in the proposed FAG-IM system. The main contributions of this paper are summarized as follows:

- We propose an innovative FA grouping-based IM transmission system, termed FAG-IM, in which ports on the FA are divided into multiple groups. Within each group, one port is selected and activated based on the information bits to transmit the modulated symbols. Then, the optimal ML detector and the linear MMSE detector are provided for the FAG-IM system.
- Based on the characteristics of the existing spatial correlation model between FA ports, a block grouping scheme is proposed where adjacent ports are assigned to the same group. We then introduce a convenient labeling scheme and establish the corresponding mapping relationship between port indices and position coordinates.
- The average bit error probability (ABEP) upper bound is derived for the FAG-IM system. Monte Carlo simulation results validate that it is a compelling theoretical tool for performance evaluation.
- The message passing structure is transplanted into the FAG-IM system. Subsequently, incorporating the structural characteristics of the transmission signal vector, an efficient structured AMP (S-AMP) detector with a linear time complexity order is proposed to reduce the receiver complexity in the FAG-IM system.
- Simulation results show that the proposed FAG-IM system exhibits strong resistance to spatial correlation, achieving superior BER performance compared to state-of-the-art systems with the same SE. Furthermore, simulation results indicate that the designed S-AMP detector significantly outperforms the MMSE detector with low complexity, thereby proving to be an efficient detector.

The rest of this paper is organized as follows: Section II presents the proposed FAG-IM system model and the spatial correlation model. Section III introduces the grouping scheme

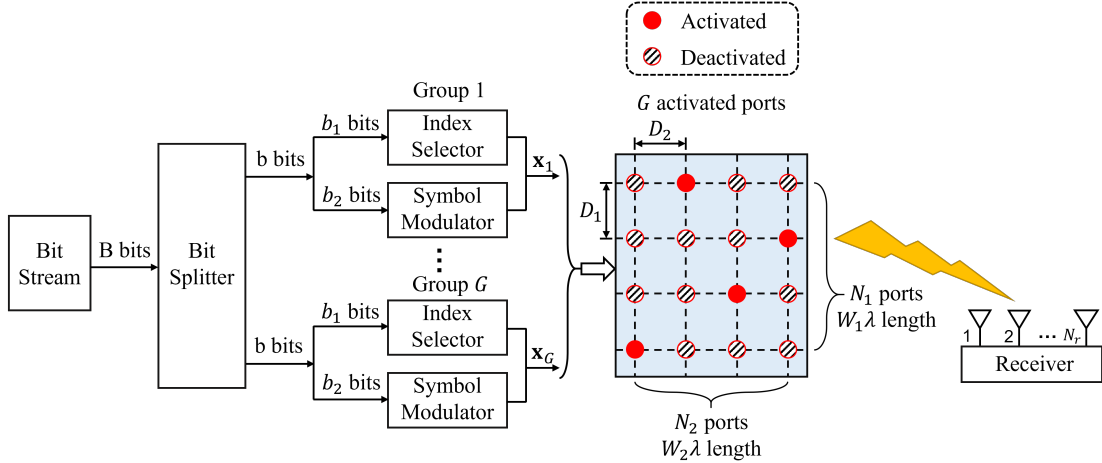


Fig. 1: Block diagram of the proposed FAG-IM system.

of FA and the corresponding mapping relationship. Section IV analyzes the theoretical performance of the proposed system. Section V establishes a message passing architecture for our system and proposes an efficient low-complexity detector. Section VI shows the simulation and comparison results. Section VII concludes this paper.

Notation: Scalar variables are denoted by italic letters, vectors are denoted by boldface small letters and matrices are denoted by boldface capital letters. $(\cdot)^*$ denotes the conjugate operation of a complex scalar variable. $\det(\cdot)$ stands for the determinant while $(\cdot)^T$, $(\cdot)^{-1}$ and $(\cdot)^H$ denote transposition, inverse and Hermitian transposition of a matrix, respectively. $|\cdot|$ and $\|\cdot\|_2$ denote the absolute and the ℓ_2 norm operations, respectively. (\cdot) and $\lfloor \cdot \rfloor$ denote the binomial coefficient and the floor operation, respectively. \otimes denotes the Kronecker product, and $\text{vec}(\cdot)$ denotes the vectorization operator. $\text{diag}(\cdot)$ denotes a diagonal matrix whose diagonal entries are the inputs. $\mathbb{E}[\cdot]$ returns the expected value of the input random quantity. The real and imaginary parts of a complex variable X are denoted by $\Re\{X\}$ and $\Im\{X\}$.

II. SYSTEM MODEL

The proposed FAG-IM system is depicted in Fig. 1. The transmitter employs a fluid antenna with N ports, while the receiver is equipped with conventional N_r FPAs. The FA occupies a two-dimensional (2D) region with an area of $\lambda W_1 \times \lambda W_2$, where λ is the wavelength of the carrier, and λW_1 and λW_2 denote the lengths of the region along the vertical and horizontal directions, respectively. Considering a grid structure, the FA has N_1 and N_2 ports uniformly distributed along the vertical and horizontal directions, respectively, with $N = N_1 \times N_2$ holding. Then, the spatial distances between adjacent ports along the vertical and horizontal directions are denoted by D_1 and D_2 , respectively, such that $D_1 = \frac{\lambda W_1}{N_1 - 1}$ and $D_2 = \frac{\lambda W_2}{N_2 - 1}$.

A. Transmission

During each transmission interval, A total of B information bits are fed into the transmitter. The transmitter then selects

and activates G ports from N ports to carry G data symbols based on these B bits.

Specifically, as shown in Fig. 1, the bit splitter divides the input B bits evenly divided into G streams, each containing b bits, i.e., $B = b \times G$. Correspondingly, the N ports on the FA are evenly divided into G groups, each containing P ports, based on a pre-designed grouping scheme (see Section III for details), such that $N = P \times G$. The b bits input to each group are further divided into two parts: b_1 and b_2 . The b_1 bits are used by the index selector to select and activate one port from P available ports. That is, the b_1 bits are transmitted by being mapped to the index of the activated port. For convenience, it is assumed in this paper that P is a power of 2, so $b_1 = \log_2 P$. The remaining b_2 bits are mapped to a data symbol using an M -ary constellation alphabet \mathbb{S} , i.e. $b_2 = \log_2 M$. Subsequently, the data symbol is transmitted through the activated port. Therefore, the SE of the proposed FAG-IM, in terms of bits per channel use (bpcu), is given by

$$\text{SE}_{\text{FAG-IM}} = B = G \times (\log_2 P + \log_2 M) \quad [\text{bpcu}]. \quad (1)$$

Denote the index set of the P available ports assigned to the g -th group by \mathbb{I}_g , where $\mathbb{I}_g \subseteq \{1, 2, \dots, N\}$ and $|\mathbb{I}_g| = P$ for $g \in \{1, 2, \dots, G\}$. The transmitted signal vector $\mathbf{x} \in \mathbb{C}^{N \times 1}$ can be represented as

$$\mathbf{x} = \sum_{g=1}^G s_g \mathbf{e}_{i_g} = \sum_{g=1}^G \mathbf{x}_g, \quad (2)$$

where $s_g \in \mathbb{S}$ denotes the g -th modulation symbol, $i_g \in \mathbb{I}_g$ denotes the index of the g -th activated port, \mathbf{e}_{i_g} denotes an N -dimensional standard basis vector with the i_g -th element being 1 and all other elements being 0, and $\mathbf{x}_g \in \mathbb{C}^{N \times 1}$ denotes the transmitted vector of the g -th group with i_g -th element being s_g and all other elements being 0.

On the other hand, the FA-IM system in [34] does not include the grouping procedure. Specifically, the information bits entering the transmitter are divided into two parts during each transmission interval. The first part is used to select and activate G ports from the total of N ports. In other words, the bits in the first part are mapped to the index of the

activated ports combination. Hence, the number of bits in the first part is $\lfloor \log_2 \binom{N}{G} \rfloor$, where $\binom{N}{G}$ denotes the total number of possible activation patterns for the FA, and the presence of the floor operation $\lfloor \cdot \rfloor$ is due to the need to satisfy the binary bit mapping relationship. The bits in the second part are modulated to G data symbols using the M -ary constellation alphabet \mathbb{S} , i.e., the number of bits in the second part is $G \times \log_2 M$. Therefore, the SE of FA-IM, in terms of bpcu, is formulated as

$$\text{SE}_{\text{FA-IM}} = \left\lfloor \log_2 \binom{N}{G} \right\rfloor + G \times \log_2 M \quad [\text{bpcu}]. \quad (3)$$

B. Spatial Correlation Model

A 2D Cartesian coordinate system with the $x-O-y$ axes is established on the plane where the FA is located. The position coordinates of the i -th port on the FA in this coordinate system is denoted as $\mathbf{t}_i = (x_i, y_i)$ for $i \in \{1, 2, \dots, N\}$. Considering a three-dimensional (3D) environment under rich scattering, the spatial correlation between the i -th port and the j -th port has been provided in [8]:

$$\begin{aligned} J_{i,j} &= \text{sinc}(k \|\mathbf{t}_i - \mathbf{t}_j\|_2) \\ &= \text{sinc} \left(k \sqrt{(x_i - x_j)^2 + (y_i - y_j)^2} \right), \end{aligned} \quad (4)$$

where $\text{sinc}(z) = \frac{\sin(z)}{z}$ and $k = \frac{2\pi}{\lambda}$. After obtaining the spatial correlation between any two ports, the spatial correlation matrix on the transmitter side can be expressed as

$$\mathbf{J}_t = \begin{bmatrix} J_{1,1} & J_{1,2} & \dots & J_{1,N} \\ J_{2,1} & J_{2,2} & \dots & J_{2,N} \\ \vdots & \vdots & \ddots & \vdots \\ J_{N,1} & J_{N,2} & \dots & J_{N,N} \end{bmatrix}. \quad (5)$$

As shown in (4), $J_{i,j} = J_{j,i}$ holds, leading to the fact that \mathbf{J}_t is a symmetric matrix. Then, \mathbf{J}_t can then be further eigen-decomposed to obtain $\mathbf{J}_t = \mathbf{U}_t \mathbf{\Lambda}_t \mathbf{U}_t^H$, where \mathbf{U}_t is an $N \times N$ matrix whose columns are the eigenvector of \mathbf{J}_t and $\mathbf{\Lambda}_t = \text{diag}(\lambda_1^t, \dots, \lambda_N^t)$ is an $N \times N$ diagonal matrix whose diagonal entries are the corresponding eigenvalues.

Taking spatial correlation into account, the channel matrix between N ports on the FA and N_r FPAs of the receiver can be modeled as

$$\mathbf{H} = \mathbf{J}_r^{\frac{1}{2}} \mathbf{G} \mathbf{J}_t^{\frac{1}{2}}, \quad (6)$$

where $\mathbf{J}_r \in \mathbb{C}^{N_r \times N_r}$ is the spatial correlation matrix on the receiver side and $\mathbf{G} \in \mathbb{C}^{N_r \times N}$ is the uncorrelated channel matrix, whose elements are i.i.d random values following $\mathcal{CN}(0, 1)$. Since \mathbf{J}_t and \mathbf{J}_r are mutually independent, and the IM mechanism is implemented only at the FA on the transmitter side, the performance difference between the proposed FAG-IM system and existing systems is primarily influenced by the spatial correlation of the transmitter side. Therefore, for simplicity, the spatial correlation on the receiver side is disregarded, i.e., $\mathbf{J}_r = \mathbf{I}_{N_r}$ is set, where \mathbf{I}_{N_r} represents the identity matrix of size N_r , consistent with the setting in [24]. Then, the channel matrix in (6) can be simplified as

$$\mathbf{H} = \mathbf{G} \sqrt{\mathbf{U}_t^H \mathbf{U}_t^H}. \quad (7)$$

C. Detection

Disregarding path loss, the received signal $\mathbf{y} \in \mathbb{C}^{N_r \times 1}$ can be written as

$$\mathbf{y} = \mathbf{H} \mathbf{x} + \mathbf{w}, \quad (8)$$

where $\mathbf{w} \in \mathbb{C}^{N_r \times 1} \sim \mathcal{CN}(0, N_0 \mathbf{I}_{N_r})$ is the additive white Gaussian noise (AWGN) vector.

Assuming the receiver has perfect knowledge of the channel state information (CSI), the optimal ML detector exhaustively attempts the possible transmitted signal vectors, which can be expressed as

$$\begin{aligned} (\hat{\mathcal{I}}, \hat{\mathbf{s}}) &= \arg \min_{\mathcal{I}, \mathbf{s}} \|\mathbf{y} - \mathbf{H} \mathbf{x}\|^2 \\ &= \arg \min_{\mathcal{I}, \mathbf{s}} \left\| \mathbf{y} - \mathbf{H} \sum_{g=1}^G s_g \mathbf{e}_{i_g} \right\|^2, \end{aligned} \quad (9)$$

where $\mathcal{I} = \{i_1, \dots, i_g, \dots, i_G\}$ represents the candidate index set of the activated ports, and $\mathbf{s} = \{s_1, \dots, s_g, \dots, s_G\}$ represents the candidate set of modulation symbols, both consisting of G elements. Although the ML detector achieves optimal detection performance, it incurs significant computational overhead and exhibits extremely high complexity.

On the other hand, the MMSE detector minimizes interference from other transmit antennas and maximizes the signal-to-interference-plus-noise ratio (SINR), which can be represented as

$$\begin{aligned} \hat{\mathbf{x}}_{\text{MMSE}} &= \mathbf{W}_{\text{MMSE}} \mathbf{y} \\ &= (\mathbf{H}^H \mathbf{H} + N_0 \mathbf{I}_N)^{-1} \mathbf{H}^H \mathbf{y}. \end{aligned} \quad (10)$$

Given $\hat{\mathbf{x}}_{\text{MMSE}}$, \hat{i}_g and \hat{s}_g can be estimated as follows

$$\hat{i}_g = \arg \max_{i \in \mathcal{I}_g} |\hat{\mathbf{x}}_{\text{MMSE}}(i)|, \quad (11)$$

$$\hat{s}_g = \arg \min_{s \in \mathbf{s}} |\hat{\mathbf{x}}_{\text{MMSE}}(\hat{i}_g) - s|, \quad (12)$$

where $\hat{\mathbf{x}}_{\text{MMSE}}(i)$ denotes the i -th element of the vector $\hat{\mathbf{x}}_{\text{MMSE}}$. Unfortunately, the linear MMSE detector still has several drawbacks. As shown in (10), the MMSE detector requires matrix inversion, which poses challenges for hardware implementation, particularly when the matrix size is large [29]. Besides, (10) is equivalent to solving a large linear system of equations, where matrix multiplication and Cholesky decomposition introduce computational complexity. Moreover, the MMSE detector has lower complexity than the ML detector, but the performance gap is notable, further enlarging under the impact of spatial correlation. In summary, an efficient low-complexity detector should be developed for the FAG-IM system, which will be elaborated in Section V.

III. GROUPING, LABELING, AND COORDINATE MAPPING

As shown in (4), given an arbitrary port index i , the position coordinates \mathbf{t}_i must be obtained to calculate the spatial correlation between ports. Accordingly, this section introduces the grouping scheme employed to mitigate spatial correlation, elaborates on how to label the ports based on the grouping results, and further provides the mapping relationship between port indices and coordinates.

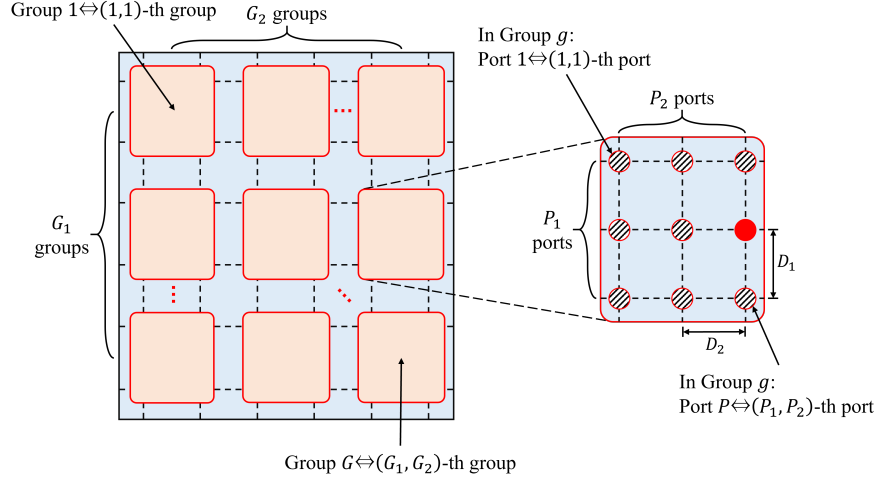


Fig. 2: Illustration of the proposed block grouping, labeling, and coordinate mapping scheme.

A. Grouping

The spatial correlation formula (4) shows that the closer the geometric distance between two ports, the stronger the spatial correlation. Considering that the working mechanism of IM involves selecting and activating ports, it is advisable to separate the activated ports as much as possible to reduce spatial correlation. Therefore, this paper adopts a block grouping scheme, as shown in Fig. 2, to partition N ports into G rectangular regions of equal size. The P ports within each region form a port group. The G index selectors of the transmitter operate independently, each selecting and activating one port from the port group it controls.

B. Labeling

A labeling method that facilitates the operation of the index selectors needs to be designed.

First, the G port groups after block partitioning are sequentially labeled in the order from top to bottom and left to right, as shown in Fig. 2. Specifically, let G_1 and G_2 represent the number of port groups along the vertical and horizontal directions, respectively, with $G = G_1 \times G_2$. The (a, b) -th group refers to the group located in the a -th row and b -th column among the G groups, where $a \in \{1, 2, \dots, G_1\}$ and $b \in \{1, 2, \dots, G_2\}$. Then, the mapping relationship between the label of the port group and its row and column numbers is given by

$$g = (b - 1)G_1 + a, \quad g \in \{1, 2, \dots, G\}. \quad (13)$$

Next, we focus on the interior of a port group. The P ports are sequentially assigned a label within the group, in the order from top to bottom and left to right, as shown in Fig. 2. Specifically, let P_1 and P_2 denote the number of ports within the group along the vertical and horizontal directions, respectively, with $P = P_1 \times P_2$. The (c, d) -th port within a group refers to the port located in the c -th row and d -th column among the P ports, where $c \in \{1, 2, \dots, P_1\}$ and $d \in \{1, 2, \dots, P_2\}$. Then, the mapping relationship between

the label assigned to a port within the group and its row and column numbers within the group is given by

$$p = (d - 1)P_1 + c, \quad p \in \{1, 2, \dots, P\}. \quad (14)$$

With the assistance of the mapping relationships (13) and (14) above, it is easy to obtain the mapping relationship between the index of a port on the FA and its corresponding group label and port label within the group, as given by

$$i = (g - 1)P + p, \quad i \in \{1, 2, \dots, N\}. \quad (15)$$

C. Coordinate Mapping

After grouping and labeling all the ports of the FA, the next step is to establish the mapping relationship between the port index and its position coordinates.

The port located at the top-left corner of the FA, i.e., the port with index $i = 1$, is chosen as the coordinate reference point \mathbf{t}_{ref} , represented as $\mathbf{t}_{\text{ref}} = \mathbf{t}_1 = (0, 0)$. Similarly, the port located at the top-left corner within the g -th group, i.e., the port indexed as $i = (g - 1)P + 1$ on the FA and labeled as $p = 1$ within the group, is chosen as the coordinate reference point $\mathbf{t}_{\text{ref}}^g$ for the group, represented as

$$\mathbf{t}_{\text{ref}}^g = \mathbf{t}_{(g-1)P+1} = \mathbf{t}_{\text{ref}} + ((a - 1)P_1 D_1, (b - 1)P_2 D_2), \quad (16)$$

where a and b are computed from the group label g using (13).

For any port on the FA, its corresponding group label g and port label p within the group are first computed from its index i using (15). Subsequently, a and b are computed from g using (13), while c and d are computed from p using (14). Finally, the position coordinates of the i -th port is expressed as

$$\begin{aligned} \mathbf{t}_i &= \mathbf{t}_{\text{ref}}^g + ((c - 1)D_1, (d - 1)D_2) \\ &= \left(((a - 1)P_1 + c - 1)D_1, ((b - 1)P_2 + d - 1)D_2 \right). \end{aligned} \quad (17)$$

Additionally, by simply setting the parameters $N_2 = G_2 = P_2 = 1$, the proposed block grouping, labeling, and coordinate mapping scheme can smoothly transfer to scenarios where the FA has a one-dimensional (1D) structure with linearly distributed ports.

TABLE I: Transmitted signal vectors of FAG-IM and FA-IM using a 1D FA with $N = 4, G = 2$.

Port index bits	FA-IM in [34]	Proposed FAG-IM
[0 0]	$[s_1, s_2, 0, 0]^T$	$[s_1, 0, s_2, 0]^T$
[0 1]	$[0, s_1, s_2, 0]^T$	$[s_1, 0, 0, s_2]^T$
[1 0]	$[0, 0, s_1, s_2]^T$	$[0, s_1, s_2, 0]^T$
[1 1]	$[s_1, 0, s_2, 0]^T$	$[0, s_1, 0, s_2]^T$

To provide a more intuitive description of the mapping relationship, the discrepancies in the transmission signal vectors between the proposed FAG-IM and the existing FA-IM are shown in Table I, where the FA is a 1D structure with $N = N_1 = 4$ and $G = 2$. Furthermore, after block grouping and labeling the ports of FAG-IM, $G_1 = G = 2$, $P = 2$, and $\mathbb{I}_1 = \{1, 2\}$, $\mathbb{I}_2 = \{3, 4\}$.

IV. PERFORMANCE ANALYSIS

This section derives a closed-form ABEP upper bound for the proposed FAG-IM system. Based on the ML detector in (9), the conditional pairwise error probability (CPEP) is given as

$$\begin{aligned} & P\{\mathcal{I} \rightarrow \hat{\mathcal{I}}, \mathbf{s} \rightarrow \hat{\mathbf{s}} \mid \mathbf{H}\} \\ &= P\{\mathbf{x} \rightarrow \hat{\mathbf{x}} \mid \mathbf{H}\} \\ &= P\left\{\|\mathbf{y} - \mathbf{Hx}\|^2 \geq \|\mathbf{y} - \mathbf{H}\hat{\mathbf{x}}\|^2\right\} \quad (18) \\ &= Q\left(\sqrt{\frac{\|\mathbf{H}\Psi\|^2}{2N_0}}\right) = Q\left(\sqrt{\frac{\Gamma}{2N_0}}\right), \end{aligned}$$

where $\Psi = \mathbf{x} - \hat{\mathbf{x}}$, $\Gamma = \|\mathbf{H}\Psi\|^2$, and $Q(\cdot)$ is the Gaussian Q -function. Based on the approximate upper bound of the Q -function [35], the CPEP can be approximated as

$$\begin{aligned} & P\{\mathcal{I} \rightarrow \hat{\mathcal{I}}, \mathbf{s} \rightarrow \hat{\mathbf{s}} \mid \mathbf{H}\} \\ & \approx \frac{1}{6} \exp\left(-\frac{\Gamma}{N_0}\right) + \frac{1}{12} \exp\left(-\frac{\Gamma}{2N_0}\right) + \frac{1}{4} \exp\left(-\frac{\Gamma}{4N_0}\right). \quad (19) \end{aligned}$$

Furthermore, the unconditional pairwise error probability (UEEP) can be expressed as

$$\begin{aligned} & P\{\mathcal{I} \rightarrow \hat{\mathcal{I}}, \mathbf{s} \rightarrow \hat{\mathbf{s}}\} \\ & \approx \frac{1}{6} M_\Gamma\left(-\frac{1}{N_0}\right) + \frac{1}{12} M_\Gamma\left(-\frac{1}{2N_0}\right) + \frac{1}{4} M_\Gamma\left(-\frac{1}{4N_0}\right). \quad (20) \end{aligned}$$

where $M_\Gamma(z) = \mathbb{E}_\Gamma[\exp(z\Gamma)]$ is the moment generating function (MGF) of Γ .

Since the format of the transmitted signal vector \mathbf{x} in (2) resembles that in conventional GSM, some of the analytical results in [36] can be integrated with some modifications to obtain

$$M_\Gamma(z) = \frac{1}{2} \frac{\exp\left(z\mathbf{u}_\mathbf{H}^H \Lambda (\mathbf{I} - z\mathbf{L}_\mathbf{H} \Lambda)^{-1} \mathbf{u}_\mathbf{H}\right)}{\det(\mathbf{I} - z\mathbf{L}_\mathbf{H} \Lambda)}, \quad (21)$$

where \mathbf{I} is the identity matrix, $\mathbf{u}_\mathbf{H} = \mathbf{u}_\mathbf{H}(\mathbf{I}_{N_r} \otimes \mathbf{J}_t)^{\frac{1}{2}} \text{vec}(\mathbf{1}_{N_r \times N})$, $\Lambda = \mathbf{I}_{N_r} \otimes \Psi\Psi^H$, and $\mathbf{L}_\mathbf{H} = \sigma_\mathbf{H}^2 \mathbf{J}_r \otimes \mathbf{J}_t$, where $\mathbf{1}_{N_r \times N}$ is an $N_r \times N$ all one matrix. Under the channel

assumptions in Section II-B, it follows that $\mathbf{u}_\mathbf{H} = 0$, $\sigma_\mathbf{H}^2 = 1$, and $\mathbf{L}_\mathbf{H} = \mathbf{I}_{N_r} \otimes \mathbf{J}_t$, hence (21) can be simplified as

$$M_\Gamma(z) = \frac{1}{2} \frac{1}{\det(\mathbf{I} - z\mathbf{J}_t \Psi \Psi^H)^{N_r}}. \quad (22)$$

The ABEP upper bound of the proposed FAG-IM system can be expressed as

$$\text{ABEP} \leq \frac{1}{2^{\text{SE}}} \sum_{\mathcal{I}, \mathbf{s}} \sum_{\hat{\mathcal{I}}, \hat{\mathbf{s}}} \frac{P\{\mathcal{I} \rightarrow \hat{\mathcal{I}}, \mathbf{s} \rightarrow \hat{\mathbf{s}}\} e(\mathcal{I} \rightarrow \hat{\mathcal{I}}, \mathbf{s} \rightarrow \hat{\mathbf{s}})}{\text{SE}}, \quad (23)$$

where $e(\mathcal{I} \rightarrow \hat{\mathcal{I}}, \mathbf{s} \rightarrow \hat{\mathbf{s}})$ represents the total number of erroneous bits for the corresponding pairwise error event.

With the simplified MGF derived from (22), substituting (20) into (23) yields (24). Note that (24) does not require numerical evaluation of integrals. Section VI will verify that the derived ABEP upper bound in (24) is a tight bound for the proposed FAG-IM system.

V. PROPOSED LOW-COMPLEXITY DETECTOR

Since the optimal ML detector jointly detects the indices of the activated ports and the symbols transmitted on them by exhaustively searching through the possible transmitted signal vectors, it is undoubtedly of high complexity. The linear MMSE detector can somewhat reduce complexity but suffers from drawbacks, such as high hardware implementation overhead and significant detection performance loss, as described in Section II-C. In this section, we first establish the message passing architecture for the FAG-IM system and then propose an efficient low-complexity decoder utilizing the AMP framework.

A. Message passing of the FAG-IM system

Based on the vector estimation problem in (8), the system can be modeled as a fully connected factor graph, which contains G variable nodes $\mathbf{v}_g, g \in \{1, 2, \dots, G\}$, and N_r observation nodes $y_r, r \in \{1, 2, \dots, N_r\}$, as illustrated in Fig. 3a.

The received signal at the r -th receive antenna can be expressed as

$$\begin{aligned} y_r &= \mathbf{h}_r \mathbf{x} + w_r \\ &= \mathbf{h}_r \sum_{g=1}^G \mathbf{x}_g + w_r \\ &= H_{r,i_g} s_g + \underbrace{\sum_{j=1, j \neq g}^G H_{r,i_j} s_j + w_r}_{\triangleq z_{rg}} \quad (25) \end{aligned}$$

where \mathbf{h}_r denotes the vector corresponding to the r -th row of matrix \mathbf{H} , H_{r,i_g} denotes the (r, i_g) -th element of \mathbf{H} , and w_r is the AWGN with zero mean and variance σ^2 . The term z_{rg} is

$$\text{ABEP} \leq \frac{1}{2^{\text{SESE}}} \sum_{\mathcal{I}, \mathbf{s}} \sum_{\hat{\mathcal{I}}, \hat{\mathbf{s}}} e(\mathcal{I} \rightarrow \hat{\mathcal{I}}, \mathbf{s} \rightarrow \hat{\mathbf{s}}) \left[\frac{1}{12} \frac{1}{\det \left(\mathbf{I} + \frac{1}{N_0} \mathbf{J}_t \Psi \Psi^H \right)^{N_r}} + \frac{1}{24} \frac{1}{\det \left(\mathbf{I} + \frac{1}{2N_0} \mathbf{J}_t \Psi \Psi^H \right)^{N_r}} + \frac{1}{8} \frac{1}{\det \left(\mathbf{I} + \frac{1}{4N_0} \mathbf{J}_t \Psi \Psi^H \right)^{N_r}} \right] \quad (24)$$

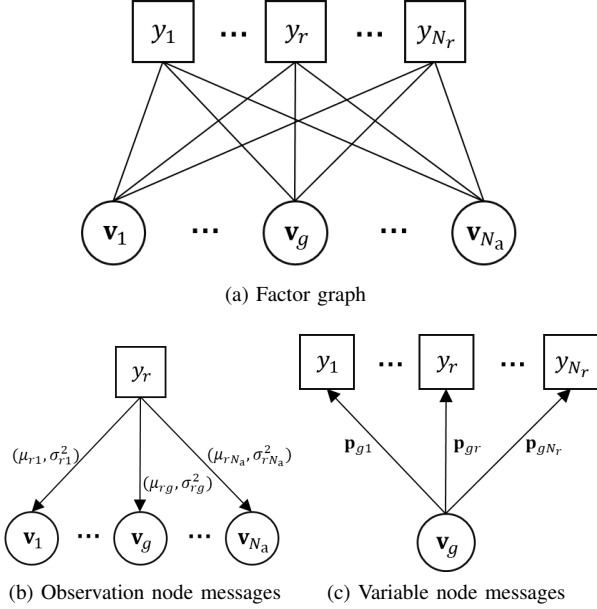


Fig. 3: The factor graph and message passing of the FAG-IM system.

approximated as following a Gaussian distribution with mean μ_{rg} and variance σ_{rg}^2 , which can be given by

$$\begin{aligned} \mu_{rg} &= \mathbb{E} \left[\sum_{j=1, j \neq g}^G H_{r,i_j} s_j + w_r \right] \\ &= \sum_{j=1, j \neq g}^G \sum_{\mathbf{x}_j} p_{jr}(\mathbf{x}_j) s_j H_{r,i_j}, \end{aligned} \quad (26)$$

$$\begin{aligned} \sigma_{rg}^2 &= \text{Var} \left[\sum_{j=1, j \neq g}^G H_{r,i_j} s_j + w_r \right] \\ &= \sum_{j=1, j \neq g}^G \sum_{\mathbf{x}_j} p_{jr}(\mathbf{x}_j) |s_j H_{r,i_j}|^2 \\ &\quad - \left| \sum_{\mathbf{x}_j} p_{jr}(\mathbf{x}_j) s_j H_{r,i_j} \right|^2 + \sigma^2, \end{aligned} \quad (27)$$

where $p_{gr}(\mathbf{x}_g)$ denotes the message transmitted from the variable node \mathbf{v}_g to the observation node y_r . The message $p_{gr}(\mathbf{x}_g)$ is given by

$$p_{gr}(\mathbf{x}_g) \propto \prod_{q=1, q \neq r}^{N_r} \exp \left(-\frac{|y_q - H_{r,i_q} s_q - \mu_{qg}|^2}{2\sigma_{qg}^2} \right). \quad (28)$$

During each iteration of the message passing algorithm, the observation node y_r computes the mean μ_{rg} and variance σ_{rg}^2 of the interference term z_{rg} and passes them as the message

to the variable node \mathbf{v}_g , as illustrated in Fig. 3b. On the other hand, the variable node \mathbf{v}_g traverses all possible values of \mathbf{x}_g to calculate the vector $\mathbf{p}_{gr} = \{p_{gr}(\mathbf{x}_g) \mid i_g \in \mathbb{I}_g, s_g \in \mathbb{S}\}$, which is then passed as the message to the observation node y_r , as illustrated in Fig. 3c. However, the message passing algorithm has high-dimensional integrations and large number of messages, leading to high computational complexity, which can impose significant overhead on practical systems.

B. Proposed S-AMP detector

Fortunately, message passing can be simplified to AMP using the Central Limit Theorem (CLT) and Taylor expansions, as discussed in [27]. In AMP, messages from a variable (factor) node to its connected factor (variable) nodes are not distinguished. Hence, the total number of messages is significantly reduced. In this subsection, we propose an efficient low-complexity S-AMP detector leveraging the structural characteristics of the transmission signal vector.

Based on the AMP framework, the vector estimation problem (8) can be decoupled into N scalar problems in the asymptotic regime, i.e.,

$$\mathbf{y} = \mathbf{Hx} + \mathbf{w} \longrightarrow \begin{cases} R_1 = x_1 + \hat{n}_1 \\ \vdots \\ R_N = x_N + \hat{n}_N, \end{cases} \quad (29)$$

where the noise $\hat{n}_i, i \in \{1, 2, \dots, N\}$, approximately follows the complex Gaussian distribution with zero mean and variance Σ_i . Define two iteration parameters

$$V_r^t = \sum_i |H_{r,i}|^2 \hat{v}_i^{t-1}, \quad (30)$$

$$Z_r^t = \sum_i H_{r,i} \hat{x}_i^{t-1} - \frac{V_r^t (y_r - Z_r^{t-1})}{\sigma^2 + V_r^{t-1}}, \quad (31)$$

where \hat{x}_i^{t-1} and \hat{v}_i^{t-1} denote the estimated posterior mean and variance of x_i , and the superscript “ t ” indicates the t -th iteration. Then, the values of Σ_i and R_i are updated by

$$\Sigma_i^t = \left[\sum_r \frac{|H_{r,i}|^2}{\sigma^2 + V_r^t} \right]^{-1}, \quad (32)$$

$$R_i^t = \hat{x}_i^{t-1} + \Sigma_i^t \sum_r \frac{H_{r,i}^* (y_r - Z_r^t)}{\sigma^2 + V_r^t}, \quad (33)$$

where $(\cdot)^*$ denotes the complex conjugate operation. With (32) and (33), the posterior distribution estimate of x_i is expressed as

$$q(x_i \mid R_i, \Sigma_i) = \frac{1}{\beta} P_0(x_i) \exp \left\{ -\frac{|x_i - R_i|^2}{\Sigma_i} \right\}, \quad (34)$$

where β represents the normalization constant, and $P_0(x_i)$ is the prior distribution of x_i . Then, \hat{x}_i^t and \hat{v}_i^t can be obtained by

$$\hat{x}_i^t = \sum_{x_i} x_i q(x_i \mid R_i^t, \Sigma_i^t), \quad (35)$$

$$\hat{v}_i^t = \sum_{x_i} |x_i|^2 q(x_i \mid R_i^t, \Sigma_i^t) - |\hat{x}_i^t|^2. \quad (36)$$

However, as indicated by (2), the transmitted signal vector \mathbf{x} in the FAG-IM system does not conform to the form $P_{\mathbf{x}}(\mathbf{x}) = \prod_{i=1}^N P_0(x_i)$, which prevents (34) from being directly applied to the data detection of FAG-IM. Additionally, the above original AMP algorithm considers general vector estimation, whereas the vectors in the FAG-IM system have sparse structural characteristics that can be exploited to enhance the detection performance. Hence, some modifications to the AMP algorithm are required to adapt to the FAG-IM system.

First, the structured priors of the vectors in the FAG-IM system are given by

$$P_{\mathbf{x}}(\mathbf{x}) = \prod_{g=1}^G P_{\mathbf{x}_g}(\mathbf{x}_g), \quad (37)$$

$$P_{\mathbf{x}_g}(\mathbf{x}_g) = \frac{1}{PM} \sum_{i \in \mathbb{I}_g} \left(\sum_{s \in \mathbb{S}} \delta(x_i - s) \prod_{j=1, j \neq i}^N \delta(x_j) \right), \quad (38)$$

where $\delta(\cdot)$ denotes the Dirac delta function. With the structured priors, (34) can be extended to the joint posterior distribution estimate of \mathbf{x}_g , which is given by

$$q(\mathbf{x}_g) \propto P_{\mathbf{x}_g}(\mathbf{x}_g) \exp \left(- \sum_{i \in \mathbb{I}_g} \frac{|x_i - R_i|^2}{\Sigma_i} \right). \quad (39)$$

Next, we derive the posterior distribution of x_i , which can only take $M + 1$ distinct values, i.e., $x_i \in \{0, \mathbb{S}\}$. Let $\mathcal{A}(i) = \{\mathbb{I}_g \mid i \in \mathbb{I}_g, g = 1, 2, \dots, G\}$ denote the index set of g -th port group, to which index i belongs. Then, the posterior distribution of x_i can be categorized into two cases:

1) Port i is activated, i.e., $x_i \in \mathbb{S}$. Based on the working mechanism of FAG-IM and (38), it can be inferred that among the P ports in the g -th group, only one port will be activated, and the activated port can only take values from set \mathbb{S} . With

(39), $q(x_i)$ can be calculated as

$$\begin{aligned} q(x_i = \alpha \mid \alpha \in \mathbb{S}) &= \frac{q(\mathbf{x}_g = \alpha \mathbf{e}_i)}{\sum_{j \in \mathcal{A}(i)} \sum_{s \in \mathbb{S}} q(\mathbf{x}_g = s \mathbf{e}_j)} \\ &= \frac{\frac{1}{PM} \exp \left(- \frac{|x_i - R_i|^2}{\Sigma_i} - \sum_{k \in \mathcal{A}(i), k \neq i} \frac{|0 - R_k|^2}{\Sigma_k} \right)}{\sum_{j \in \mathcal{A}(i)} \sum_{s \in \mathbb{S}} \frac{1}{PM} \exp \left(- \frac{|s - R_j|^2}{\Sigma_j} - \sum_{k \in \mathcal{A}(i), k \neq j} \frac{|0 - R_k|^2}{\Sigma_k} \right)} \\ &= \frac{\exp \left(- \frac{|x_i|^2 - 2\Re\{x_i^* R_i\}}{\Sigma_i} - \sum_{k \in \mathcal{A}(i)} \frac{|R_k|^2}{\Sigma_k} \right)}{\sum_{j \in \mathcal{A}(i)} \sum_{s \in \mathbb{S}} \exp \left(- \frac{|s|^2 - 2\Re\{s^* R_j\}}{\Sigma_j} - \sum_{k \in \mathcal{A}(i)} \frac{|R_k|^2}{\Sigma_k} \right)} \\ &= \frac{\exp \left(- \frac{|x_i|^2 - 2\Re\{x_i^* R_i\}}{\Sigma_i} \right)}{\sum_{j \in \mathcal{A}(i)} \sum_{s \in \mathbb{S}} \exp \left(- \frac{|s|^2 - 2\Re\{s^* R_j\}}{\Sigma_j} \right)}. \end{aligned} \quad (40)$$

2) Port i is not activated, i.e., $x_i = 0$. With (40), $q(x_i = 0)$ can be written as

$$\begin{aligned} q(x_i = 0) &= 1 - \sum_{s \in \mathbb{S}} q(x_i = s) \\ &= 1 - \frac{\sum_{s \in \mathbb{S}} \exp \left(- \frac{|s|^2 - 2\Re\{s^* R_i\}}{\Sigma_i} \right)}{\sum_{j \in \mathcal{A}(i)} \sum_{s \in \mathbb{S}} \exp \left(- \frac{|s|^2 - 2\Re\{s^* R_j\}}{\Sigma_j} \right)}. \end{aligned} \quad (41)$$

By substituting (40) and (41) into (35) and (36), the posterior mean and variance estimates of x_i in the FAG-IM system can be obtained as

$$\begin{aligned} \hat{x}_i^t &= \sum_{s \in \mathbb{S}} s \times q(x_i = s) + 0 \times q(x_i = 0) \\ &= \frac{\sum_{s \in \mathbb{S}} s \exp \left(- \frac{|s|^2 - 2\Re\{s^* R_i^t\}}{\Sigma_i^t} \right)}{\sum_{j \in \mathcal{A}(i)} \sum_{s \in \mathbb{S}} \exp \left(- \frac{|s|^2 - 2\Re\{s^* R_j^t\}}{\Sigma_j^t} \right)}, \end{aligned} \quad (42)$$

$$\begin{aligned} \hat{v}_i^t &= \sum_{s \in \mathbb{S}} |s|^2 \times q(x_i = s) + 0^2 \times q(x_i = 0) - |\hat{x}_i^t|^2 \\ &= \frac{\sum_{s \in \mathbb{S}} |s|^2 \exp \left(- \frac{|s|^2 - 2\Re\{s^* R_i^t\}}{\Sigma_i^t} \right)}{\sum_{j \in \mathcal{A}(i)} \sum_{s \in \mathbb{S}} \exp \left(- \frac{|s|^2 - 2\Re\{s^* R_j^t\}}{\Sigma_j^t} \right)} - |\hat{x}_i^t|^2. \end{aligned} \quad (43)$$

Moreover, aggressive message updates may sometimes lead to the divergence of the proposed S-AMP detector. We employ the widely used damping mechanism to tackle this issue and enhance the stability of the detector [37]. After introducing damping in the S-AMP algorithm, the update equations (30) and (31) of V_r^t and Z_r^t are modified to

$$V_r^t = \Delta \cdot \sum_i |H_{r,i}|^2 \hat{v}_i^{t-1} + (1 - \Delta) \cdot V_r^{t-1}, \quad (44)$$

$$Z_r^t = \Delta \cdot \left[\sum_i H_{r,i} \hat{x}_i^{t-1} - \frac{V_r^t (y_r - Z_r^{t-1})}{\sigma^2 + V_r^{t-1}} \right] + (1 - \Delta) \cdot Z_r^{t-1}, \quad (45)$$

Algorithm 1 Proposed S-AMP detector for the FAG-IM system

Input:

Received signal \mathbf{y} ;
 Equivalent channel matrix \mathbf{H} ;
 Constellation alphabet \mathbb{S} ;
 Complex Gaussian noise variance σ^2 ;
 Damping factor Δ ;
 Maximum number of iterations T_{\max} ;
 Iteration termination threshold ε_{th} .

Output: $\hat{\mathbf{x}}^L$.

```

1: Iteration initialization:  $\hat{x}_i^0 = 0$ ,  $\hat{v}_i^0 = 1/P$ ,  $i = 1, \dots, N$ ,  

    $V_r^0 = 1/P$ ,  $Z_r^0 = 0$ ,  $r = 1, \dots, N_r$ .  

2: for  $t = 1, \dots, T_{\max}$ , do  

3:   for  $r = 1, \dots, N_r$ , do  

4:     Update  $V_r^t$  according to (44);  

5:     Update  $Z_r^t$  according to (45);  

6:   end for  

7:   for  $i = 1, \dots, N$ , do  

8:     Update  $\Sigma_i^t$  according to (32);  

9:     Update  $R_i^t$  according to (33);  

10:  end for  

11:  for  $i = 1, \dots, N$ , do  

12:    Update  $\hat{x}_i^t$  according to (42);  

13:    Update  $\hat{v}_i^t$  according to (43);  

14:  end for  

15:   $L \leftarrow t$ ;  

16:  if  $\|\hat{\mathbf{x}}^t - \hat{\mathbf{x}}^{t-1}\|^2 / \|\hat{\mathbf{x}}^t\|^2 \leq \varepsilon_{\text{th}}$  then  

17:    break;  

18:  end if  

19: end for

```

where $\Delta \in (0, 1]$ is the damping factor used to adjust the convergence speed.

The steps of the proposed low-complexity S-AMP detector are described in **Algorithm 1**. Firstly, initialize the parameters required for the iteration. Then, the values of the relevant parameters are updated iteratively based on the derived computational equations until the maximum number of iterations is reached or the stopping criterion is satisfied. Finally, output the value of $\hat{\mathbf{x}}^L = [\hat{x}_1^L, \dots, \hat{x}_N^L]^T$ as the final estimate of \mathbf{x} , where L denotes the number of iterations upon termination.

C. Complexity analysis

Based on **Algorithm 1**, each iteration in the proposed S-AMP detector involves the computational updates of V_r^t , Z_r^t , Σ_i^t , R_i^t , \hat{x}_i^t , and \hat{v}_i^t . Specifically, according to (44) and (45), the complexity order of updating V_r^t and Z_r^t is $\mathcal{O}(N_r N)$. According to (32) and (33), the complexity order of updating Σ_i^t and R_i^t is $\mathcal{O}(N N_r)$. While computing \hat{x}_i^t , examining the denominator term in (42), it can be noted that for $\forall j \in \mathcal{A}(i), j \neq i$, $\mathcal{A}(j) = \mathcal{A}(i)$ always holds. Consequently, the denominator term of each \hat{x}_j^t is identical to that of \hat{x}_i^t , so it only needs to be computed once. Hence, the complexity order of updating \hat{x}_i^t is $\mathcal{O}(NM)$. According to (43), the complexity order of computing \hat{v}_i^t is $\mathcal{O}(NM)$, similar to the analysis for

\hat{x}_i^t . Therefore, when the algorithm terminates after L iterations, the overall complexity order of the proposed S-AMP detector is $\mathcal{O}(LN N_r + LN M)$.

In comparison, the complexity order of the ML detector under the FAG-IM system is $\mathcal{O}(P^G M^G N N_r)$, and the complexity order of the MMSE detector is $\mathcal{O}(N^3 + N^2 N_r)$. Meanwhile, the complexity order of the ML detector in the FA-IM system is $\mathcal{O}(2^{\lfloor \log_2 \binom{N}{G} \rfloor} M^G N N_r)$ [34]. In summary, it can be concluded that the complexity order of the ML detector under the FAG-IM system is lower than that of the ML detector under the FA-IM system, implying that the FAG-IM system is inherently more suitable for implementing low-complexity detection than the FA-IM system. More excitingly, the proposed S-AMP detector, devised by exploiting the unique structural characteristics of the transmission signal vector under the FAG-IM system, significantly reduces the complexity order from exponential to linear. This further amplifies the advantage of FAG-IM over FA-IM.

VI. SIMULATION RESULTS

In this section, the simulation results are presented to evaluate the performance of the proposed FAG-IM system, validate the derived ABEP upper bound, and assess the performance of the S-AMP detector designed for the FAG-IM system. In the comparative simulation, the channel model used for all schemes is described in Section II, where path loss is neglected, and receivers are assumed to have perfect knowledge of CSI.

First, under the same SE, the BER performance of the proposed FAG-IM system is compared with that of the state-of-the-art FA-IM system in [34], as shown in Fig. 4. Both systems employ BPSK modulation and the optimal ML detector. The parameters associated with the FA are configured as $W_1 = 2$, $W_2 = 4$, $N = N_1 \times N_2 = 2 \times 4 = 8$, $G = G_1 \times G_2 = 1 \times 2 = 2$, yielding the same SE, i.e., $\text{SE}_{\text{FAG-IM}} = \text{SE}_{\text{FA-IM}} = 6$ bpcu. Meanwhile, the number of receive antennas N_r is varied to examine the effect on the performance of both systems. As observed from Fig. 4, increasing N_r results in higher receive diversity gain, leading to improvement in the BER performance of both systems. However, regardless of the number of receive antennas, the proposed FAG-IM system consistently demonstrates superior BER performance. Specifically, when the BER reaches the level of 10^{-4} , compared to the FA-IM system, the proposed FAG-IM system can provide signal-to-noise-ratio (SNR) gains of approximately 0.59 dB, 0.42 dB, 0.39 dB, and 0.32 dB for $N_r = 2, 4, 8$, and 16, respectively. Consequently, the proposed FAG-IM system achieves higher SNR gains as the number of receive antennas decreases. Besides, Fig. 4 plots the ABEP curves for the above configuration, calculated using (24). It can be observed that the derived theoretical upper bound closely matches the Monte Carlo simulation results, particularly in the high SNR regions.

Subsequently, Fig. 5 further compares the BER performance of the proposed FAG-IM system with the FA-IM system under various levels of spatial correlation strength, along with

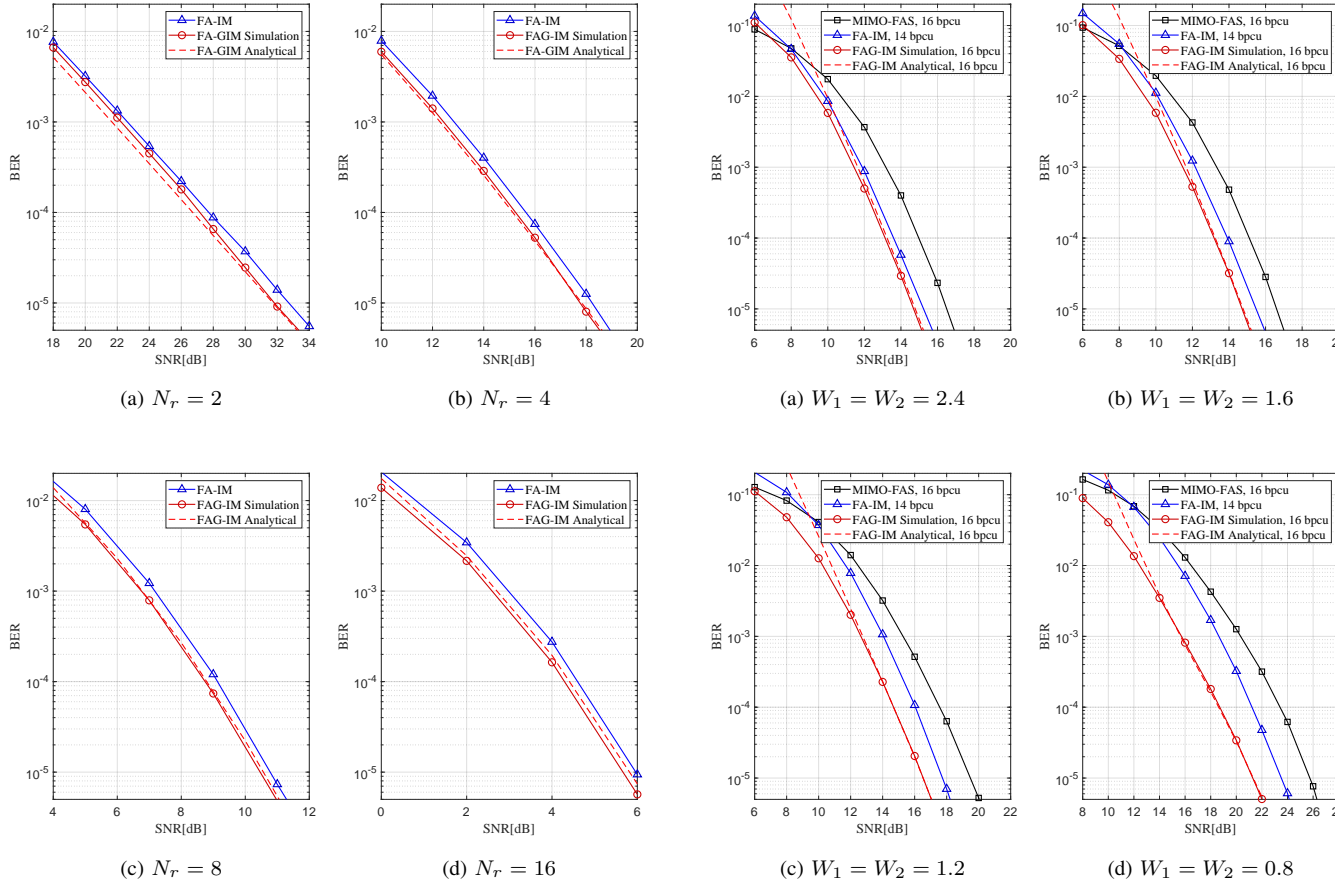


Fig. 4: BER performance comparisons between the proposed FAG-IM system and the FA-IM system with different N_r . $W_1 = 2, W_2 = 4, N = N_1 \times N_2 = 2 \times 4 = 8, G = G_1 \times G_2 = 1 \times 2 = 2, \text{SE}_{\text{FAG-IM}} = \text{SE}_{\text{FA-IM}} = 6 \text{ bpcu}$.

comparisons to the conventional MIMO-FAS system¹ in [17]. The spatial correlation strength can be controlled by adjusting the spatial distances D_1 and D_2 between adjacent ports. Therefore, in the simulations, W_1 and W_2 are varied while keeping N_1 and N_2 constant. The parameters related to the FA are set as $N = N_1 \times N_2 = 4 \times 4 = 16, G = G_1 \times G_2 = 2 \times 2 = 4$, and all systems employ the ML detector with $N_r = 8$. To enable comparison under approximately the same SE, the FAG-IM, FA-IM, and MIMO-FAS systems use 4-QAM, BPSK, and 16-QAM constellations, respectively, with corresponding SEs of $\text{SE}_{\text{FAG-IM}} = \text{SE}_{\text{MIMO-FAS}} = 16 \text{ bpcu}$ and $\text{SE}_{\text{FA-IM}} = 14 \text{ bpcu}$. As observed from Fig. 5, as W_1 and W_2 decrease, i.e., as the spatial correlation strength increases, the SNR gain offered by the proposed FAG-IM system becomes larger. Notably, when the BER reaches the 10^{-4} level, the FAG-IM system offers SNR gains of 0.47 dB, 0.76 dB, 1.41 dB, and 2.55 dB compared to the FA-IM system and gains of 1.87 dB, 1.94 dB, 2.92 dB, and 4.73 dB compared to the MIMO-FAS system for

¹The conventional MIMO-FAS system, unlike the FAG-IM and FA-IM systems that select and activate ports based on bits, selects the optimal ports for bit transmission based on the CSI, meaning that the port indices do not carry any information.

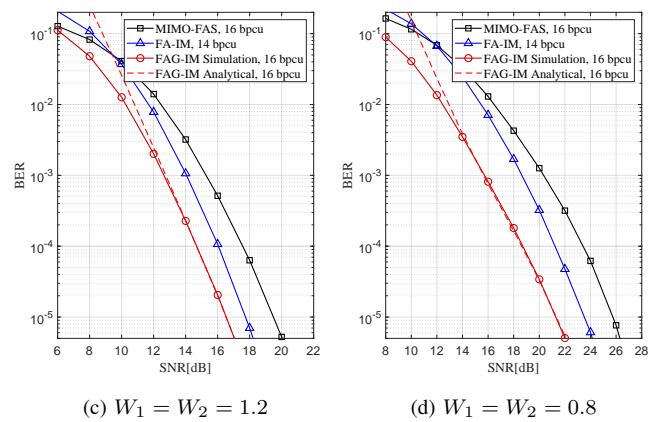


Fig. 5: BER comparison results of the proposed FAG-IM, FA-IM, and MIMO-FAS systems under different levels of spatial correlation strength. $N = N_1 \times N_2 = 4 \times 4 = 16, G = G_1 \times G_2 = 2 \times 2 = 4, N_r = 8$.

$W_1 = W_2 = 2.4, 1.6, 1.2, 0.8$, respectively. It is worth noting that the FA-IM system is configured with a lower SE of 14 bpcu, which implies that, at the same SE, the FAG-IM system would provide a greater SNR gain. In conclusion, the spatial correlation between the FA ports on the transmitter side makes it more challenging for the receivers of the FA-IM and MIMO-FAS systems to distinguish between different transmission patterns, leading to performance degradation. In contrast, the proposed FAG-IM system effectively mitigates the impact of spatial correlation, with the improvement becoming more significant as the correlation strength increases. Therefore, the FAG-IM system is an efficient and robust transmission system. In addition, Fig. 5 also illustrates the theoretical ABEP curves of the FAG-IM system, which fit well with the simulation results in the high SNR region. Therefore, both Fig. 4 and Fig. 5 indicate that the derived ABEP upper bound can serve as a powerful theoretical tool for assessing system performance.

Next, the performance of the S-AMP detector, tailored for the FAG-IM system, is evaluated. In all subsequent experiments, based on our experience, the damping factor of the S-AMP detector is set to $\Delta = 0.9$, the maximum number of iterations is set to $T_{\max} = 15$, and the iteration termination

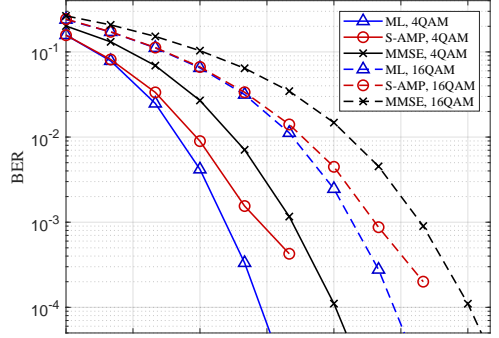
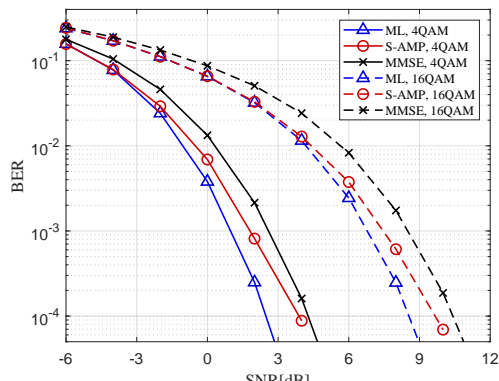
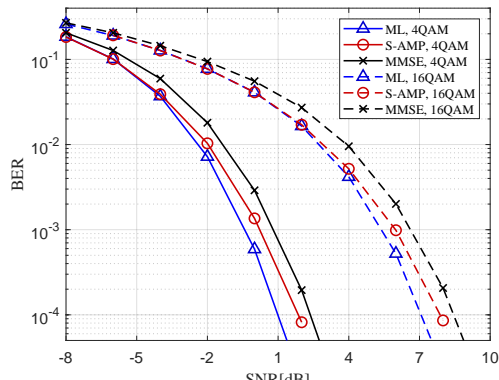
(a) $N_r = 16$ (b) $N_r = 24$ (c) $N_r = 32$

Fig. 6: BER performance of the FAG-IM system with different detectors under different modulation orders and different N_r , $W_1 = 2$, $W_2 = 4$, $N = N_1 \times N_2 = 2 \times 4 = 8$, $G = G_1 \times G_2 = 1 \times 2 = 2$.

threshold is set to $\varepsilon_{th} = 10^{-16}$.

Fig. 6 investigates the BER performance of the FAG-IM system using the proposed S-AMP detector, the optimal ML detector, and the MMSE detector under different modulation orders M and varying numbers of receive antennas N_r . The parameters associated with the FA are configured as $W_1 =$

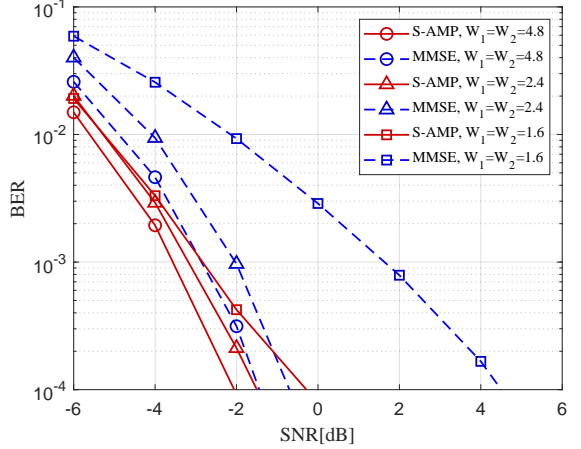


Fig. 7: BER performance comparison of the proposed S-AMP and MMSE detectors under different levels of spatial correlation strength. 4-QAM , $N = N_1 \times N_2 = 4 \times 4 = 16$, $G = G_1 \times G_2 = 2 \times 2 = 4$, $N_r = 128$.

2 , $W_2 = 4$, $N = N_1 \times N_2 = 2 \times 4 = 8$, $G = G_1 \times G_2 = 1 \times 2 = 2$. Fig. 6 shows that at a BER of 10^{-3} with 4-QAM modulation, the performance gap between S-AMP and ML is 2.69 dB, 0.85 dB, and 0.65 dB, while the SNR gain over MMSE is 1.46 dB, 0.76 dB, and 0.57 dB for $N_r = 16, 24, 32$, respectively. With 16-QAM modulation, the performance gap between S-AMP and ML is 1.01 dB, 0.79 dB, and 0.63 dB, while the SNR gain over MMSE is 2.02 dB, 0.95 dB, and 0.64 dB for $N_r = 16, 24, 32$, respectively. It can be summarized that as N_r increases, the performance of the S-AMP detector approaches that of the ML detector while the SNR gain over the MMSE detector diminishes. On the other hand, an increase in M not only makes the performance of the S-AMP detector closer to that of the ML detector but also enlarges the SNR gain over the MMSE detector.

Fig. 7 compares the BER performance of the FAG-IM system with the S-AMP and MMSE detectors under different levels of spatial correlation strength, i.e., for different values of W_1 and W_2 . The FAG-IM system employs 4-QAM modulation, with the other parameters configured as $N = N_1 \times N_2 = 4 \times 4 = 16$, $G = G_1 \times G_2 = 2 \times 2 = 4$, $N_r = 128$. As shown in Fig. 7, with the increase in spatial correlation strength, i.e., as W_1 and W_2 decrease, the BER performance gain of the proposed S-AMP detector over the MMSE detector becomes more significant. To be precise, when the BER reaches the 10^{-3} level, the S-AMP detector provides SNR gains of 0.71 dB, 1.61 dB, and 4.45 dB compared to the MMSE detector, for $W_1 = W_2 = 4.8, 2.4, 1.6$, respectively. Therefore, it can be concluded that the S-AMP detector exhibits superior robustness to spatial correlation compared to the MMSE detector.

Finally, the impact of the number of activated ports G on the S-AMP detector performance is investigated, as illustrated in Fig. 8. In this case, the FAG-IM system employs 4-QAM modulation with $N_r = 64$. To minimize interference from factors such as spatial correlation, the FAG-IM system is equipped

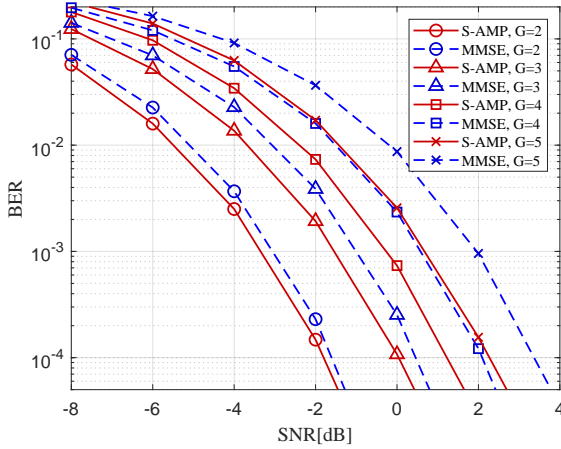


Fig. 8: The BER performance of the S-AMP and MMSE detectors for different numbers of activated ports G . 1D FA, $D_1 = 1.2\lambda$, $P = 4$, $N = P \cdot G = 4G$, 4QAM, $N_r = 64$.

with a 1D FA. The spatial distance between adjacent ports is fixed at $D_1 = 1.2\lambda$, and the number of ports allocated to each group is set to $P = 4$, while the number of groups G is varied, resulting in $N = P \cdot G = 4G$. Figure 8 demonstrates that as the number of activated ports increases, the performance gain provided by the proposed S-AMP detector becomes more significant. Specifically, at a BER level of 10^{-3} , the S-AMP detector achieves SNR gains of 0.31 dB, 0.55 dB, 0.85 dB, and 1.27 dB compared to the MMSE detector for $G = 2, 3, 4, 5$, respectively. Overall, the proposed S-AMP detector not only facilitates a reduction in receiver complexity for the FAG-IM system but also significantly outperforms the MMSE detector in terms of BER performance, thereby validating its effectiveness as a low-complexity, high-efficiency detector.

VII. CONCLUSION

This paper proposes a novel FA grouping-based IM system, termed FAG-IM, to mitigate the effects of spatial correlation between ports. Leveraging the spatial correlation model of the FA and considering the port distribution structure, the proposed FAG-IM system employs a block grouping scheme, where adjacent ports are assigned to the same group. A practical port labeling scheme is provided in this context, and the mapping relationship between port indices and coordinates is established. Subsequently, the theoretical ABEP upper bound is derived, showing excellent agreement with the simulation results, which indicates that it can serve as an effective tool for assessing the performance of the proposed FAG-IM system. In order to reduce receiver complexity, the message passing architecture is first introduced into the FAG-IM system. Then, by exploiting the structural properties of the transmission signal vector and integrating the AMP algorithm, we propose the S-AMP detector, which reduces the time complexity order to a linear scale. The simulation results validate that the proposed FAG-IM system demonstrates greater robustness under the influence of spatial correlation compared to the FA-IM system. The simulation results also indicate that the proposed

low-complexity S-AMP detector significantly outperforms the MMSE detector in terms of BER performance.

REFERENCES

- [1] Y. Xu, N. Gao, H. Hong, Y. Cai, X. Duan, D. He, Y. Wu, and W. Zhang, “Enhancements on coding and modulation schemes for LTE-based 5G terrestrial broadcast system,” *IEEE Trans. Broadcast.*, vol. 66, no. 2, pp. 481–489, 2020.
- [2] H. Hong, Y. Xu, Y. Wu, D. He, N. Gao, and W. Zhang, “Backward compatible low-complexity demapping algorithms for two-dimensional non-uniform constellations in ATSC 3.0,” *IEEE Trans. Broadcast.*, vol. 67, no. 1, pp. 46–55, 2021.
- [3] X. Guo, Y. Xu, N. Zhang, L. Xin, D. He, W. Zhang, and Y.-Y. Wu, “NUC optimization design for multi-layer layered division multiplexing,” in *Proc. IEEE Int. Symp. Broadband Multimedia Syst. Broadcast. (BMSB)*, 2024, pp. 1–5.
- [4] X. Ou, Y. Xu, H. Hong, D. He, Y. Wu, Y. Huang, and W. Zhang, “A DRL-based joint scheduling and resource allocation scheme for mixed unicast–broadcast transmission in 5G,” *IEEE Trans. Broadcast.*, vol. 69, no. 3, pp. 661–674, 2023.
- [5] R. Liu, Y. Xu, Y. Wu, D. He, W. Zhang, and C. W. Chen, “Detecting abrupt channel changes for IRS-assisted MIMO communication,” *IEEE Wireless Commun. Lett.*, vol. 13, no. 1, pp. 29–33, 2024.
- [6] K.-K. Wong, A. Shojaeifard, K.-F. Tong, and Y. Zhang, “Fluid antenna systems,” *IEEE Trans. Wireless Commun.*, vol. 20, no. 3, pp. 1950–1962, 2021.
- [7] L. Zhu, W. Ma, and R. Zhang, “Modeling and performance analysis for movable antenna enabled wireless communications,” *IEEE Trans. Wireless Commun.*, vol. 23, no. 6, pp. 6234–6250, 2024.
- [8] W. K. New, K.-K. Wong, H. Xu, C. Wang, F. R. Ghadi, J. Zhang, J. Rao, R. Murch, P. Ramírez-Espinosa, D. Morales-Jimenez, C.-B. Chae, and K.-F. Tong, “A tutorial on fluid antenna system for 6G networks: Encompassing communication theory, optimization methods and hardware designs,” *IEEE Commun. Surveys Tuts.*, pp. 1–1, 2024.
- [9] L. Zhu, W. Ma, and R. Zhang, “Movable antennas for wireless communication: Opportunities and challenges,” *IEEE Commun. Mag.*, vol. 62, no. 6, pp. 114–120, 2024.
- [10] Y. Huang, L. Xing, C. Song, S. Wang, and F. Elhouni, “Liquid antennas: Past, present and future,” *IEEE Open J. Antennas Propag.*, vol. 2, pp. 473–487, 2021.
- [11] S. Basbug, “Design and synthesis of antenna array with movable elements along semicircular paths,” *IEEE Antennas Wireless Propag. Lett.*, vol. 16, pp. 3059–3062, 2017.
- [12] W. C. Jakes and D. C. Cox, *Microwave Mobile Communications*. Wiley-IEEE Press, 1994.
- [13] P. Ramírez-Espinosa, D. Morales-Jimenez, and K.-K. Wong, “A new spatial block-correlation model for fluid antenna systems,” *IEEE Trans. Wireless Commun.*, pp. 1–1, 2024.
- [14] Z. Chai, K.-K. Wong, K.-F. Tong, Y. Chen, and Y. Zhang, “Port selection for fluid antenna systems,” *IEEE Commun. Lett.*, vol. 26, no. 5, pp. 1180–1184, 2022.
- [15] L. Tlebaldiyeva, G. Nauryzbayev, S. Arzykulov, A. Eltawil, and T. Tsiftsis, “Enhancing QoS through fluid antenna systems over correlated Nakagami- m fading channels,” in *Proc. IEEE Wireless Commun. Netw. Conf. (WCNC)*, 2022, pp. 78–83.
- [16] L. Zhu, W. Ma, B. Ning, and R. Zhang, “Movable-antenna enhanced multiuser communication via antenna position optimization,” *IEEE Trans. Wireless Commun.*, vol. 23, no. 7, pp. 7214–7229, 2024.
- [17] W. K. New, K.-K. Wong, H. Xu, K.-F. Tong, and C.-B. Chae, “An information-theoretic characterization of MIMO-FAS: Optimization, diversity-multiplexing tradeoff and q -outage capacity,” *IEEE Trans. Wireless Commun.*, vol. 23, no. 6, pp. 5541–5556, 2024.
- [18] J. Jeganathan, A. Ghrayeb, L. Szczecinski, and A. Ceron, “Space shift keying modulation for MIMO channels,” *IEEE Trans. Wireless Commun.*, vol. 8, no. 7, pp. 3692–3703, 2009.
- [19] E. Basar, M. Wen, R. Mesleh, M. Di Renzo, Y. Xiao, and H. Haas, “Index modulation techniques for next-generation wireless networks,” *IEEE Access*, vol. 5, pp. 16 693–16 746, 2017.
- [20] R. Y. Mesleh, H. Haas, S. Sinanovic, C. W. Ahn, and S. Yun, “Spatial modulation,” *IEEE Trans. Veh. Technol.*, vol. 57, no. 4, pp. 2228–2241, 2008.
- [21] X. Guo, Y. Xu, H. Hong, S. Peng, D. He, W. Zhang, and Y.-Y. Wu, “Design of capacity-approaching constellation and pre-scaling for spatial modulation,” in *Proc. IEEE Veh. Technol. Conf. (Spring)*, 2024, pp. 1–5.

- [22] T. Lakshmi Narasimhan, P. Raviteja, and A. Chockalingam, "Generalized spatial modulation in large-scale multiuser MIMO systems," *IEEE Trans. Wireless Commun.*, vol. 14, no. 7, pp. 3764–3779, 2015.
- [23] A. Younis, N. Serafimovski, R. Mesleh, and H. Haas, "Generalised spatial modulation," in *Proc. IEEE Conf. Rec. 44th Asilomar Conf. Signals, Syst. Comput.*, 2010, pp. 1498–1502.
- [24] W. Qu, M. Zhang, X. Cheng, and P. Ju, "Generalized spatial modulation with transmit antenna grouping for massive MIMO," *IEEE Access*, vol. 5, pp. 26798–26807, 2017.
- [25] M. D. Renzo, H. Haas, and P. M. Grant, "Spatial modulation for multiple-antenna wireless systems: a survey," *IEEE Commun. Mag.*, vol. 49, no. 12, pp. 182–191, 2011.
- [26] A. Garcia-Rodriguez and C. Masouros, "Low-complexity compressive sensing detection for spatial modulation in large-scale multiple access channels," *IEEE Trans. Commun.*, vol. 63, no. 7, pp. 2565–2579, 2015.
- [27] D. L. Donoho, A. Maleki, and A. Montanari, "Message passing algorithms for compressed sensing: I. motivation and construction," in *Proc. IEEE Inf. Theory Work. Inf. Theory*, 2010, pp. 1–5.
- [28] S. Wang, Y. Li, M. Zhao, and J. Wang, "Energy-efficient and low-complexity uplink transceiver for massive spatial modulation MIMO," *IEEE Trans. Veh. Technol.*, vol. 64, no. 10, pp. 4617–4632, 2015.
- [29] S. Wang, Y. Li, and J. Wang, "Multiuser detection in massive spatial modulation MIMO with low-resolution ADCs," *IEEE Trans. Wireless Commun.*, vol. 14, no. 4, pp. 2156–2168, 2015.
- [30] X. Meng, S. Wu, L. Kuang, D. Huang, and J. Lu, "Multi-user detection for spatial modulation via structured approximate message passing," *IEEE Commun. Lett.*, vol. 20, no. 8, pp. 1527–1530, 2016.
- [31] E. Faddoul, Y. Guo, G. M. Kraidy, C. Psomas, and I. Krikidis, "Correlation mitigation schemes for index-modulated fluid antenna systems," in *Proc. IEEE Global Commun. Conf. (GLOBECOM)*, 2023, pp. 5324–5329.
- [32] Y. Chen and T. Xu, "Fluid antenna index modulation communications," *IEEE Wireless Commun. Lett.*, vol. 13, no. 4, pp. 1203–1207, 2024.
- [33] H. Yang, H. Xu, K.-K. Wong, C.-B. Chae, R. Murch, S. Jin, and Y. Zhang, "Position index modulation for fluid antenna system," *IEEE Trans. Wireless Commun.*, vol. 23, no. 11, pp. 16773–16787, 2024.
- [34] J. Zhu, G. Chen, P. Gao, P. Xiao, Z. Lin, and A. Quddus, "Index modulation for fluid antenna-assisted MIMO communications: System design and performance analysis," *IEEE Trans. Wireless Commun.*, pp. 1–1, 2024.
- [35] M. Chiani, D. Dardari, and M. Simon, "New exponential bounds and approximations for the computation of error probability in fading channels," *IEEE Trans. Wireless Commun.*, vol. 2, no. 4, pp. 840–845, 2003.
- [36] A. Younis, R. Mesleh, M. Di Renzo, and H. Haas, "Generalised spatial modulation for large-scale MIMO," in *Proc. Eur. Signal Process. Conf. (EUSIPCO)*, 2014, pp. 346–350.
- [37] M. Petti, "A message-passing algorithm with damping," *J. Statist. Mech., Theory Exp.*, vol. 2005, no. 11, p. P11008, nov 2005.